Comparison of microwave satellite humidity data and radiosonde profiles: A case study

S. A. Buehler, M. Kuvatov, and V. O. John
Institute of Environmental Physics, University of Bremen, Bremen, Germany

U. Leiterer and H. Dier
Meteorological Observatory Lindenberg, German Weather Service, Lindenberg, Germany

Received 5 February 2004; revised 7 April 2004; accepted 3 May 2004; published 2 July 2004.

[1] This article documents a case study comparing radiosonde humidity data to Advanced Microwave Sounding Unit (AMSU) satellite humidity data. The study had two goals: first, to develop a robust method for such a comparison, and second, to check the quality and mutual consistency of radiosonde data, radiative transfer model, and AMSU data. The radiosonde data used are Vaisala RS80 data from the station Lindenberg of the German Weather Service (DWD), which have been subject to several corrections compared to the standard data processing. The radiative transfer model is the Atmospheric Radiative Transfer Simulator (ARTS), and the AMSU data are those of the satellites NOAA 15 and 16 for the time periods 2001 and 2002. The comparison was done in radiance space, using a radiative transfer model to simulate AMSU radiances from the radiosonde data. The overall agreement is very good, with radiance biases below 1.5 K and standard deviations below 2 K. The main source of "noise" in the comparison is atmospheric inhomogeneity on the 10-km scale. While the radiosonde correction performed at Lindenberg significantly reduces the bias between simulated and measured AMSU radiance, there still remains a slope in the radiance difference. Possible reasons for this were investigated. Most likely, the radiosondes underestimate the relative humidity under extremely dry conditions, showing 0 %RH when the true value is 2–4 %RH. *INDEX TERMS:* 1655 Global Change: Water cycles (1836); 3360 Meteorology and Atmospheric Dynamics: Remote sensing; 3394 Meteorology and Atmospheric Dynamics: Instruments and techniques; *KEYWORDS:* humidity, radiosonde, AMSU

Citation: Buehler, S. A., M. Kuvatov, V. O. John, U. Leiterer, and H. Dier (2004), Comparison of microwave satellite humidity data and radiosonde profiles: A case study, *J. Geophys. Res.*, *109*, D13103, doi:10.1029/2004JD004605.

1. Introduction

[2] Upper tropospheric humidity (UTH) is a crucial parameter for meteorology and climate research [*Spencer and Braswell*, 1997; *Bates et al.*, 2001; *Soden and Bretherton*, 1993; *Harries*, 1997]. There are two global and continuous data sets for this parameter, one from polar-orbiting meteorological sensors and the other from synoptic meteorological radiosondes.

[3] The satellite data come from two series of satellites, one from the National Oceanic and Atmospheric Administration (NOAA) and the other from the Defense Meteorological Satellite Program (DMSP). UTH is measured by infrared instruments at 6.7 μm [*Soden and Lanzante*, 1996; *Soden et al.*, 2004], and by microwave instruments at 183 GHz [*Engelen and Stephens*, 1998]. This article focuses on the microwave measurements. They have the advantage of being much less affected by clouds than the infrared measurements. These data are used operationally by the numerical weather prediction (NWP) community, which has developed NWP-model-based tools to monitor satellite radiometer performance [*Atkinson*, 2000], valuable for identifying intersatellite differences and changes over time, but problematic if one is interested in absolute UTH. Operational products are generated by NOAA/National Environmental Satellite Data and Information Service, which also routinely perform radiosonde intercomparison activities [*Reale et al.*, 2003].

[4] Microwave humidity data exist from Special Sensor Microwave Water Vapor Sounder (SSM-T2) on the DMSP satellites, from Advanced Microwave Sounding Unit (AMSU-B) on the NOAA satellites, and from Humidity Sounder for Brazil (HSB) on the Aqua satellite. Information on the available data is summarized in Table 1. This study focuses on NOAA 15 and NOAA 16 for the years 2001–2002. The AMSU data can be downloaded from the Satellite Active Archive.

[5] The synoptic radiosonde data go back to the 1940s [*Elliot and Gaffen*, 1991]. Records are kept at meteorological agencies. Data can be obtained, for example, from the British Atmospheric Data Centre (BADC). There are about 850 stations in the data record at the BADC, but only about 250 stations have at least 10 launches per month reaching

Copyright 2004 by the American Geophysical Union.
0148-0227/04/2004JD004605$09.00

Table 1. A Summary of Currently Operating Microwave Satellite Humidity Sensors

Platform Name	Instrument Name	Launch
DMSP F-13	SSM-T2	March 1995
DMSP F-14	SSM-T2	April 1997
NOAA 15 (NOAA K)	AMSU-B	May 1998
NOAA 16 (NOAA L)	AMSU-B	September 2000
NOAA 17 (NOAA M)	AMSU-B	June 2002
Aqua	HSB	May 2002

100 hPa. Ideally, each station should launch a radiosonde 4 times a day at the synoptic observation times 0000, 0600, 1200, and 1800 UTC. However, many stations only launch sondes irregularly. The quality of the data from the different stations is also believed to vary considerably.

[6] For this case study it was decided to focus on the radiosonde data from one station, the reference station Lindenberg of the German Weather Service (DWD). This has the advantages that the properties and quality of the data are well understood and that high-vertical-resolution data, which are not in the BADC archive, can be used.

[7] The basic idea of the study is to compare satellite and radiosonde data. However, the satellite measures radiances, not humidity directly. While obtaining radiances from given temperature and humidity profiles is straightforward, obtaining humidity concentrations from radiances is complicated and requires additional assumptions (a classical inverse problem [*Rodgers*, 2000]). To avoid having to deal with the inverse problem, the comparison is done in radiance space rather than state space: A radiative transfer (RT) model is used to generate simulated satellite measurements from the radiosonde data, which can then be compared to the real satellite measurements. This approach has already been used for infrared data, for example, by *Soden and Lanzante* [1996], but has so far not been used for microwave data as far as we know.

[8] The aims of the study are as follows: first, to develop a robust methodology for such a comparison, second, to check the mutual consistency of (1) satellite data, (2) radiosonde data, and (3) RT model, and third, to check the mutual consistency and stability of instruments on different satellites. Another aim is to pave the way for a systematic comparison of all stations in the global radiosonde network to satellite data. This will allow an intercomparison and quality control of the different radiosonde stations, assuming that the satellite instrument's properties are stable during a few orbits.

[9] The structure of the article is as follows: Section 2 presents the satellite and radiosonde data, focusing on those data properties that are relevant for the comparison. Section 3 presents the RT model, the method of finding matches between the two data sets, and the error model. Section 4 discusses the results for different instrument channels, different radiosonde qualities, and different satellite instruments, and section 5 summarizes the conclusions.

2. Data

2.1. Lindenberg Radiosonde Data

[10] The Meteorological Observatory Lindenberg, located at 52°22′N, 14°12′E, is one of the reference stations of the DWD. The radiosonde record there goes back to 1905. Recently, strong efforts have been made to improve the calibration of Humicap humidity sensors [*Leiterer et al.*, 1997], together with the manufacturer Vaisala.

[11] Figure 1 shows two high-resolution radiosonde profiles, corresponding to the driest and wettest days in the year 2002 (5 January and 17 July, respectively). Note the fine vertical structures in the humidity profile. Humidity values exceeding the ice saturation line in the lower plot are indicative of the presence of cirrus clouds. Three versions of the same radiosonde data were used in this study, high-resolution uncorrected (HRNC), high-resolution corrected (HRC), and low-resolution corrected (LRC).

[12] Version HRNC is data treated by the standard Vaisala processing method and should therefore correspond to high-resolution data from other stations using Vaisala RS80 humidity sensors. Version HRC is data corrected to high-quality research sondes, which are launched at Lindenberg once a week. The corrections applied are described in detail by *Leiterer et al.* [1997]. There are three corrections: dry bias correction, detection and elimination of data affected by sensor icing, and time lag correction. Over the whole year 2002, the integrated water vapor content between 500 and 200 hPa is 3.33% higher for the corrected data (0.721 kg m^{-2} compared to 0.697 kg m^{-2}). The average UTH (average relative humidity between 500 and 200 hPa) is 3.4 %RH higher for the corrected data (35.3 %RH compared to 31.9 %RH).

[13] Version LRC of the data is the low-resolution data that are broadcasted in the operational radiosonde network. From the approximately 300 altitude levels of the high-resolution data between the surface and 100 hPa, only 30 "significant" levels remain. This procedure leads to a loss of detail, but only to a very small bias of 0.25 %RH. It has to be pointed out that this good agreement between LRC and HRC data can only be achieved if the LRC data are interpolated to a fine grid before calculating column quantities. The interpolation scheme is crucial; the best results are obtained when humidity is interpolated in relative humidity, whereas interpolation of humidity in volume mixing ratio leads to a large discrepancy between the two data sets.

[14] It is important to understand these biases since (uncorrected) low-resolution data are all that is readily available for most of the radiosonde stations worldwide, which will be affected by a dry bias from the missing sensor correction.

2.2. AMSU-B Data

[15] Details on the AMSU-B instrument can be found in an article by *Saunders et al.* [1995]. It is a cross-track scanning microwave sensor with channels at 89.0, 150.0, 183.31 ± 1.00, 183.31 ± 3.00, and 183.31 ± 7.00 GHz. These channels are called channels 16–20 of the overall AMSU instruments; channels 1–15 belong to AMSU-A. The instrument has a swath width of approximately 2300 km, which is sampled at 90 scan positions. The satellite viewing angle for the innermost scan positions is 0.55° from nadir; for the outermost scan positions it is 48.95° from nadir. This corresponds to incidence angles of 0.62° and 58.5° from nadir, respectively. The footprint size is 20 × 16 km^2 for the innermost scan positions but increases to 64 × 52 km^2 for the outermost positions.

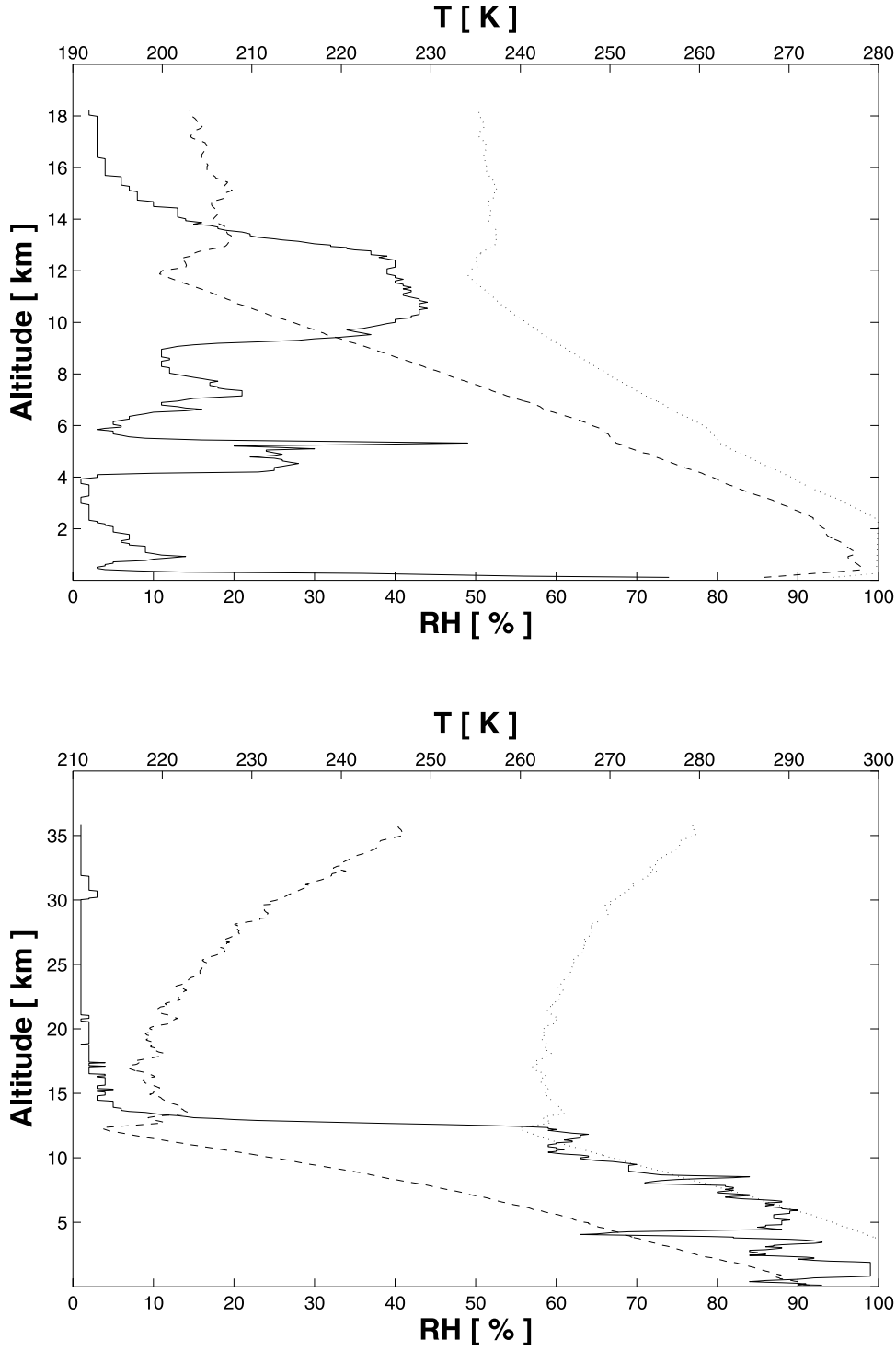

Figure 1. Lindenberg radiosonde profiles. (top) Driest day, 5 January 2002; (bottom) wettest day, 17 July 2002. The solid line is relative humidity (with respect to liquid water), the dashed line is temperature, and the dotted line is the relative humidity corresponding to ice saturation.

Figure 2 shows an example of AMSU data from channel 20. This is an overpass over the station Lindenberg.

[16] Figure 3 shows the AMSU-B channel frequency positions relative to the atmospheric zenith opacity spectrum. Channels 16 and 17 are surface channels. The interesting channels for this study are channels 18–20, which sample the free troposphere. The sampling altitude for each channel can best be seen from the Jacobian [*Rodgers*, 2000], i.e., the derivative of the channel radiance with respect to a change in local atmospheric humidity. Examples are displayed in Figure 4. Note that the Jacobians move significantly with changing atmospheric state. In particular, channel 20, which normally cannot see the surface, can see the surface under very dry conditions.

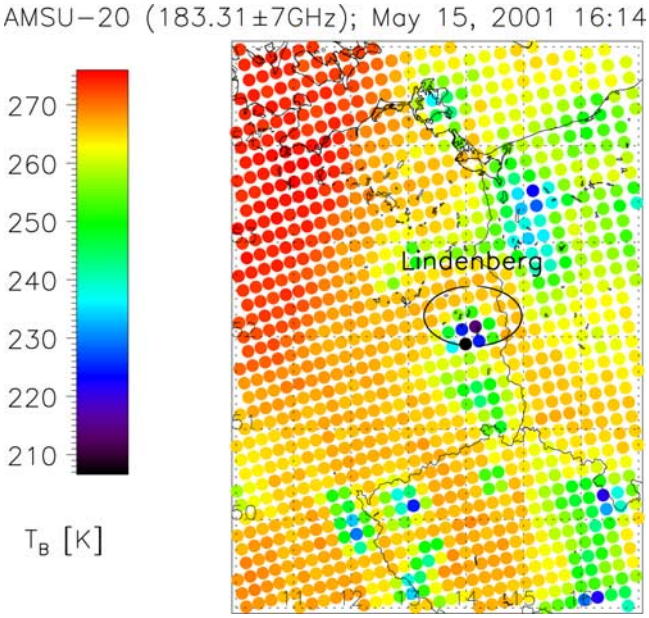

Figure 2. An AMSU overpass over station Lindenberg. The circle drawn around the station has a radius of 50 km.

[17] Each NOAA satellite passes Lindenberg 2 times a day. Figure 5 shows histograms of the overpass times (in UTC) of NOAA 15 and 16 for the year 2002.

3. Methodology

3.1. Radiative Transfer

[18] The RT model Atmospheric Radiative Transfer Simulator (ARTS), described in an article by *Buehler et al.* [2004], was used to simulate AMSU radiances on the basis of radiosonde profiles. Five radiance values, one for each AMSU-B channel, were obtained for each radiosonde launch. Radiances were expressed as brightness temperatures in Kelvin, similar to the AMSU data. The program setup for this study was as follows:

[19] Gaseous absorption was assumed to be only due to water vapor, oxygen, and nitrogen. Absorption models used were that of *Rosenkranz* [1998] for water vapor and oxygen and that of *Rosenkranz* [1993] for nitrogen. For the radiative transfer calculation, temperature and relative humidity were interpolated linearly in log pressure onto 1000 pressure levels, evenly spaced in log pressure, between the surface

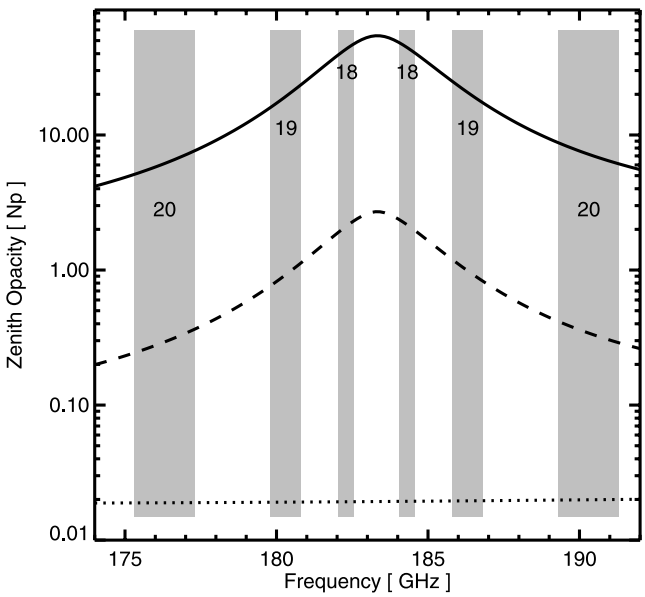

Figure 3. Atmospheric zenith opacity as a function of frequency. AMSU-B channel positions for the three humidity channels are indicated. The dashed and solid opacity curves correspond to the driest and wettest Lindenberg radiosonde profiles displayed in Figure 1. The dotted line is the dry air opacity. The grey shaded areas indicate the bandwidth of the channels.

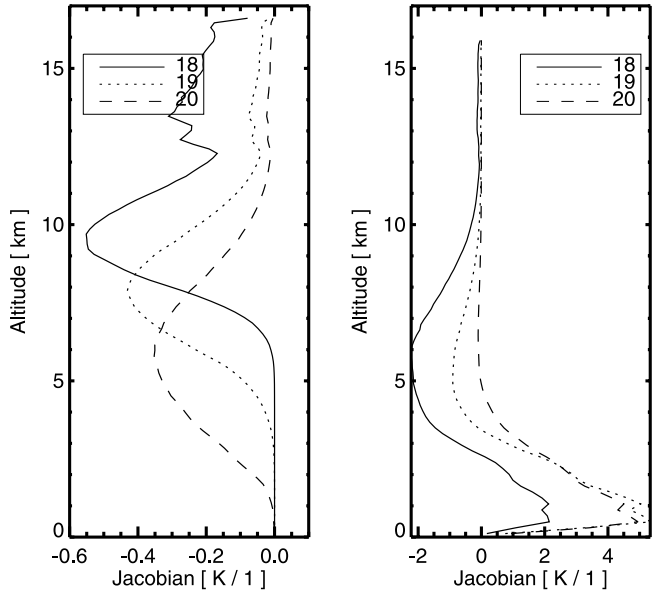

Figure 4. AMSU-B humidity Jacobians in fractional units. These units are such that the values correspond to the change in brightness temperature for a doubling of the mixing ratio at one grid point. (left) For wettest Lindenberg radiosonde profile; (right) for driest profile.

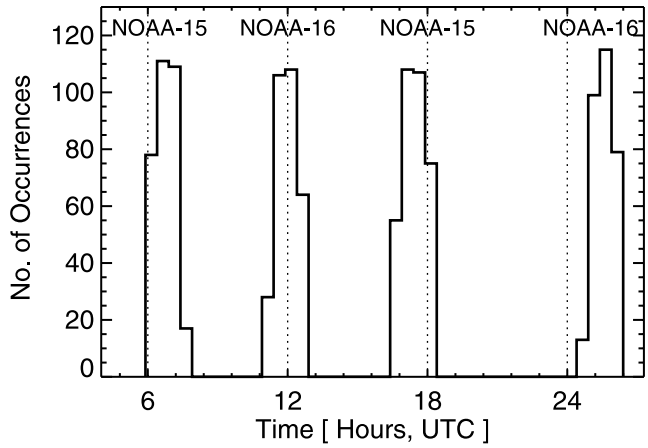

Figure 5. Histograms of NOAA satellite overpass times. These are the times when an AMSU-B pixel closer than 25 km to the station occurred. The dotted vertical lines represent synoptic hours.

Table 2. Difference in Millikelvin Between Simulated Brightness Temperatures for Profiles Cut at 100 hPa and Full Profiles Up to 10 hPa (Mean and Standard Deviation)[a]

Channel	GN	GON	MN	MON
16	1 ± 42	32 ± 74	−30 ± 34	−33 ± 57
17	12 ± 19	32 ± 29	−7 ± 15	0 ± 26
18	81 ± 31	130 ± 57	60 ± 25	90 ± 47
19	27 ± 9	46 ± 16	18 ± 6	31 ± 11
20	20 ± 9	38 ± 14	10 ± 8	23 ± 10

[a]GN, global profiles, nadir view; GON, global profiles, most off-nadir view; MN, midlatitude profiles, nadir view; MON, midlatitude profiles, most off-nadir view. Midlatitude means that only profiles between 50° and 70°N were used. In most cases, the cut profiles result in slightly warmer brightness temperatures.

and 100 hPa. The radiative transfer integration step along the line of sight was 5 m, and the platform altitude 850 km. Atmospheric refraction was turned off; it has negligible impact for these satellite viewing angles. The geometric altitude profile was taken from the radiosonde data. Monochromatic calculations were performed for 11 frequencies inside the passbands, and the results were convolved with the sensor passband response, which was assumed to be rectangular. It was also tested whether a Gaussian passband response would lead to significant differences, but brightness temperature differences were well below 0.1 K. It would be preferable to use measured passband responses, but unfortunately no such measurements are currently available for AMSU-B (N. Atkinson, personal communication, 2003).

[20] Required geophysical inputs of the model in this case are humidity and temperature profiles, the surface emissivity, and the surface skin temperature. Humidity and temperature profiles were taken from the radiosonde, the surface emissivity was assumed fix at 0.95, and the skin temperature was assumed to be equal to the lowest radiosonde temperature. The surface emissivity influences mainly window channels 16 and 17 and, under extremely dry conditions, also channel 20. Channels 18 and 19 are not influenced by the surface, which was found by repeating the analysis, as described below, for different surface emissivity values. That exercise also confirmed the choice of 0.95 for the surface emissivity as reasonable for the Lindenberg area.

[21] Radiosondes do not always reach the same altitude. In order to eliminate the influence of the different maximum altitudes, all profiles were cut at 100 hPa, an altitude reached by all but 406 sondes in the 2001–2002 time period. Of course, this cutting introduces both a bias (from the missing dry atmosphere above 100 hPa) and a random error (from temperature and humidity fluctuations above 100 hPa). Simulations for the European Centre for Medium-Range Weather Forecasts data set [*Chevallier*, 2001] were used to assess this. These profiles go up to 10 hPa. The difference between simulations with the full profile and the profile cut at 100 hPa are summarized in Table 2. The cutting procedure mainly introduces a bias of approximately −0.033 to 0.090 K, depending on channel, but only a small random error of 0.006–0.057 K.

3.2. Selecting Matches

[22] Given a radiosonde profile, one can simulate an AMSU measurement. However, how to compare this to the real AMSU data? Matching the sonde to an individual AMSU pixel would be overambitious, if only because the sonde drifts approximately 50 km horizontally during its ascent to 100 hPa. Hence our approach is to compare the sonde to the average AMSU radiance in a target area, described by a circle of radius 50 km (compare Figure 2). Normally, 10–30 pixels will be in this target area.

[23] Since the AMSU data in the target area are taken under different satellite viewing angles, the limb effect has to be considered. Off-nadir radiances will be slightly lower than nadir radiances for channels 18–20 and slightly higher for channels 16 and 17. This behavior is called limb darkening and limb brightening, respectively. Figure 6 shows the effect for all AMSU-B channels for the mean atmospheric state of the Lindenberg HRC 2002 data set. The effect is due to the longer path length that the radiation travels through each atmospheric layer for an off-nadir viewing angle. For upper tropospheric channels 18–20 this shifts the sounding altitude upward, where the atmosphere is colder. For surface channels 16 and 17 it leads to increased atmospheric emissions that add to the (colder) surface radiation.

[24] From Figure 6 one can estimate that the magnitude of the limb effect within the target area is less than approximately 1 K. In principle, the correct approach for the simulations would be to simulate radiances for the different satellite viewing angles and average. However, for simplicity, we simulate the radiance only for the viewing angle corresponding to the center of the circle. Because of nonlinearities this introduces an error, which we estimate to be 1 order of magnitude less than the limb effect itself, and therefore negligible.

[25] The next problem is the satellite overpass time, which can be up to 3 hours before or after the radiosonde launch (see Figure 5). The displacement of the air mass measured by the sonde during this time is estimated as follows: First, the average wind speed and direction between 700 and 300 hPa are calculated from the radiosonde wind data. These two pressure altitudes correspond to the peaks of the channel 20 and 18 Jacobians for a Lindenberg mean profile; hence this altitude range is most important for the humidity channels.

[26] The average wind vector is then multiplied by the time difference between the satellite overpass and half an hour before the synoptic time. In the ideal case the sonde should be launched approximately 1 hour before the synoptic time, so that the synoptic time is representative for the profile as a whole. Therefore the time difference between overpass and half an hour before the synoptic time is the appropriate one to use. If the displacement calculated in this way is larger than 50 km, the data are discarded. This eliminates approximately 35% of the matches.

3.3. Error Model

[27] Sources of error for the comparison are as follows: (1) radiometric noise of the AMSU measurement, (2) sampling error due to atmospheric inhomogeneity, (3) radiosonde measurement error in humidity and temperature, (4) RT model error (systematic), and (5) AMSU calibration error.

[28] The concept of the target area can be used to estimate the combined effect of error sources 1 and 2, by calculating $\sigma_{50\mathrm{km}}(i)$, the standard deviation of the brightness temperature

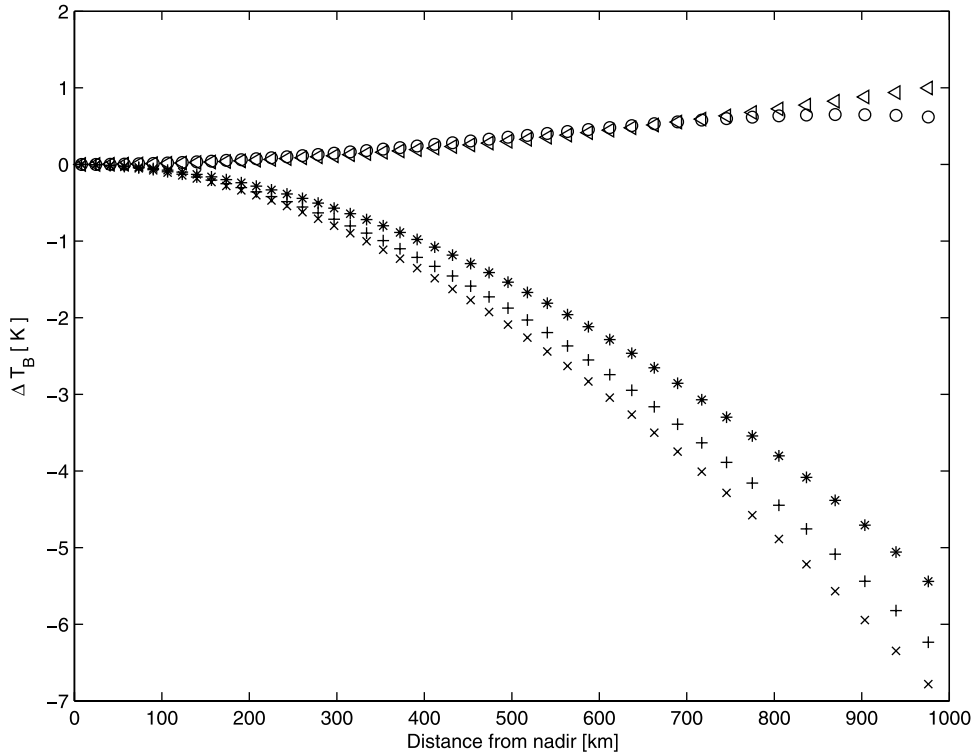

Figure 6. Limb darkening or brightening as a function of distance from nadir for channel 16 (triangles), 17 (circles), 18 (crosses), 19 (plusses), and 20 (asterisks).

of all pixels within the target area. The index *i* here indicates that this can be calculated for every match. Figure 7 shows histograms of this quantity for the year 2002 for both satellites.

[29] If the atmosphere is very homogeneous, σ_{50km} should be determined by the radiometric noise, as expressed by the noise equivalent temperature σ_{RN}, plus a small contribution from the limb effect. This is confirmed by the good agreement of the σ_{RN} estimated from the AMSU calibration (vertical lines in Figure 7) with the left edge of the histograms. Channel 16, and to a lesser degree 17, are exceptions, since for these channels the inhomogeneity of the surface plays a significant role. Figure 7 also confirms that the performance of channel 18 has greatly improved for NOAA 16 compared to NOAA 15. Channel 19 has also slightly improved.

[30] If σ_{50km} is significantly above the radiometric noise, it means that atmospheric inhomogeneities on the 15–50 km scale are present. The σ_{50km} can exceed 4 K; in most cases it will be the dominant error source. This suggests the error model

$$\sigma(i) = C_0 + \sigma_{50km}(i) \quad (1)$$

[31] A χ^2 test for a linear fit of AMSU radiances versus ARTS simulated radiances, in combination with a goodness of fit estimate [*Press et al.*, 1992, equation 15.2.12], was used to try this error model for different values of the constant C_0. For this, the matches were divided into different σ_{50km} bins, and χ^2 and probability Q were calculated for each bin. Figure 8 shows the results for channel 19 of NOAA 15 for the full year of 2001.

[32] If $C_0 = 0$, only the cases with rather high σ_{50km} have a reasonably low χ^2 and hence a reasonably high probability Q. This confirms that for low inhomogeneity the other error sources contribute significantly.

[33] Plots similar to Figure 8 were made for channels 18–20 for both satellites and years, resulting in a total of 12 plots. To keep the error model simple, a global constant value of $C_0 = 0.5$ K was selected as giving a reasonable probability for all cases. This constant is assumed to account for error sources 3, 4, and 5 and also for that part of the sampling error 2 that is due to inhomogeneities on a smaller scale than is resolved by AMSU. This places 0.5 K upper bounds on the RT model error 4 and the AMSU calibration error 5. It also places an upper bound of approximately 5% on the radiosonde humidity error, which can be derived by sensitivity RT calculations. (Here we mean a radiosonde calibration error that is fixed for one launch but random between different launches.)

[34] As an example of the level of agreement that can be achieved, Figure 9 shows scatterplots of AMSU radiance versus ARTS modeled radiance for AMSU-B channels 18–20 on NOAA 15 for the year 2001.

3.4. Cirrus Cloud Filtering

[35] Another issue to be addressed is a possible contamination of the measurement by cirrus cloud scattering. From model calculations by *Sreerekha et al.* [2002] this is expected to be only significant for strong cirrus clouds. In that case, one expects the measured radiances to be colder than the simulated ones, because the cloud scatters radiation out of the line of sight of the instrument. The most sensitive channel for this effect is channel 20, because its Jacobian peaks below typical cirrus cloud altitudes.

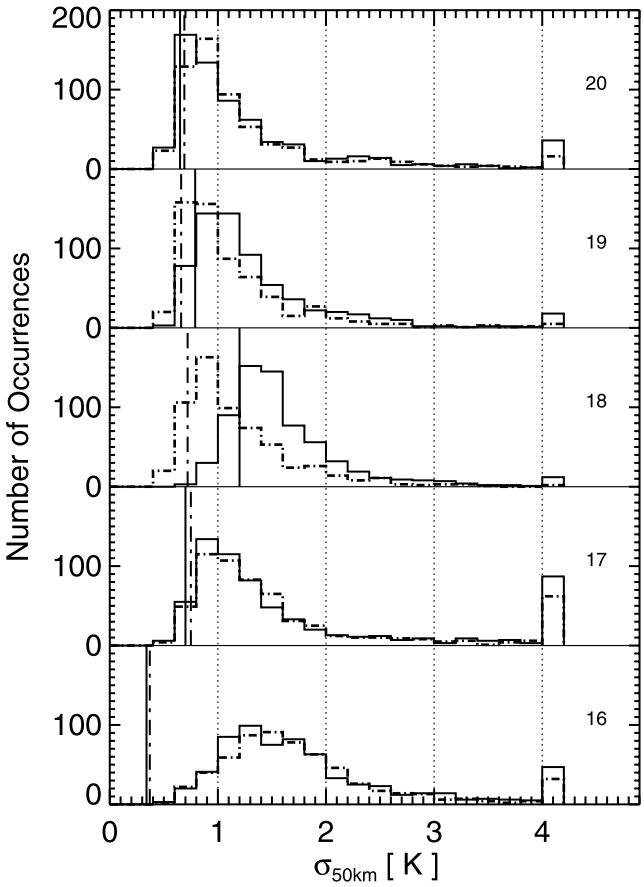

Figure 7. Histograms of target area average radiance standard deviation, σ_{50km}, for all AMSU-B channels. The channel is indicated in the right part of each figure. The solid line represents NOAA 15 data for 2002, and the dash-dotted line represents NOAA 16 data for the same year. The rightmost bin contains all data for which $\sigma_{50km} > 4$ K. The vertical solid and dash-dotted lines indicate the mean noise equivalent temperatures (σ_{RN}) from the instrument calibration process, also for the same year, which were derived from 10-day median values (courtesy of the Met Office, UK).

[36] We define D as the difference between measured and modeled radiances:

$$D(i) = T_B^{AMSU}(i) - T_B^{ARTS}(i), \quad (2)$$

where i is again the index of the match. Figure 10 shows a scatterplot of D^{20}, the difference between measurement and model for channel 20, as a function of $T_B^{AMSU-20}$, the measured radiance in channel 20. At $T_B^{AMSU-20}$ below approximately 260 K the measured radiances start to get significantly colder than the modeled ones. We interpret this behavior as the cloud signal. Because the present study uses only a clear-sky RT model, all matches with $T_B^{AMSU-20} <$ 260 K are discarded, thus implementing a rough filter against strong ice clouds. Although only channel 20 is used to define the filter, it is applied to all channels.

[37] The results are not very sensitive to the exact value of the cloud filter threshold. For example, the bias between radiosonde and satellite data for channel 18 (see section 3.5 for exact definition) will change by only 0.2 K when the cloud filter threshold is varied from 255 K to 265 K. Most of this change happens between 260 K and 265 K, because at these high threshold values a significant part of the data is removed by the filter. The slope between modeled and measured radiances (see also section 3.5 for definition) is even less affected by the threshold value: It changes only by 0.02 K/K when the threshold value is varied from 255 K to 265 K.

3.5. Statistics

[38] The mean value $\bar{D}$ of the differences $D(i)$ could be taken to represent the bias between the modeled and the measured radiances. However, it is more appropriate to define a measure of the bias that takes into account the error model as described in section 3.4. Hence we define the bias B as

$$B = \frac{\sum \sigma(i)^{-2} D(i)}{\sum \sigma(i)^{-2}}. \quad (3)$$

As pointed out by *Soden and Bretherton* [1993], radiance differences scale in proportion to relative errors in relative

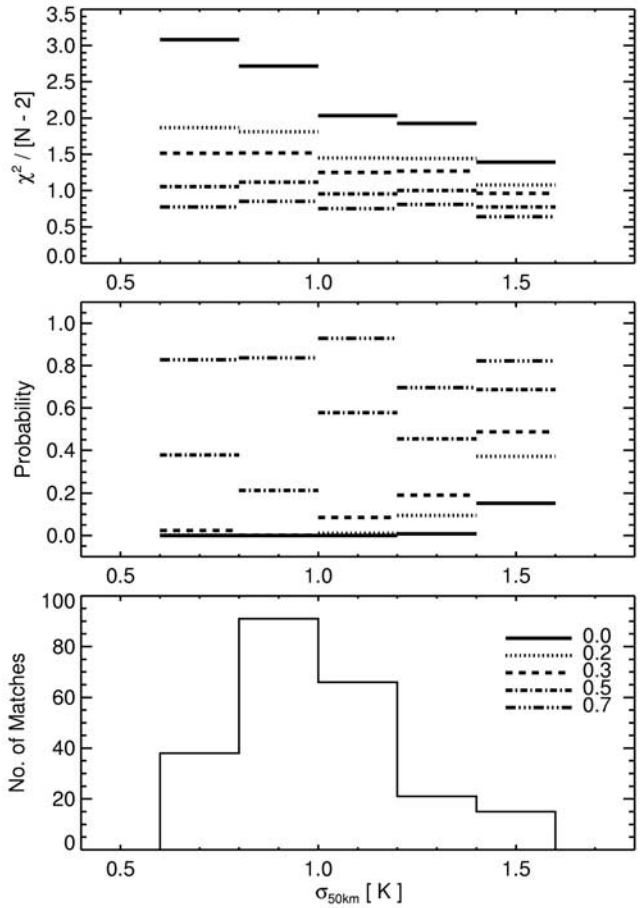

Figure 8. Result of χ^2 test for the credibility of the error model. The top plot shows the χ^2 values normalized to $N - 2$ for each bin, where N is the number of matches for each bin. The middle plot shows the probability, which gives a quantitative measure of the goodness of fit of the model. The bottom plot shows the number of matches in each bin. Line styles used for different C_0 values are shown in the bottom plot.

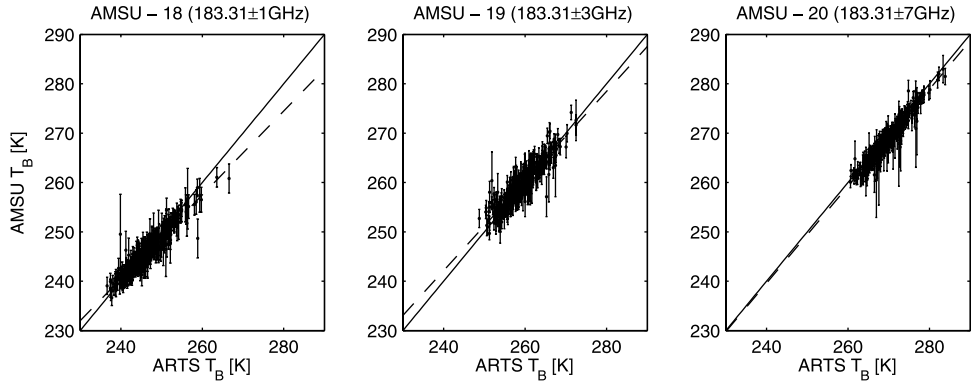

Figure 9. Average AMSU radiance for a 50-km-radius target area versus ARTS modeled radiance based on radiosonde data. Time period, 2002; satellite, NOAA 15; data set, HRC; number of points in the plot, 290. Vertical bars indicate the $\sigma(i)$ as defined in equation (1). The dashed line is a linear fit. Panels from left to right are for channels 18–20.

humidity. In the case of channel 18, a bias B of 1 K in brightness temperature corresponds to approximately 10% relative error in relative humidity, as shown in Figure 11. It is important to note that the sensitivity depends on the temperature profile rather than on the humidity level; therefore the figure shows curves for several different temperature profiles. The sensitivity is displayed for relative changes in relative humidity, using 50 %RH as the reference. The sensitivity is highest for the high-lapse-rate temperature profile.

[39] The uncertainty in the bias can be estimated from its standard deviation

$$\sigma_B = \sqrt{\frac{1}{\sum \sigma(i)^{-2}}}. \quad (4)$$

[40] Figure 9 suggests that in some channels there may be not only a bias but also a slope between modeled and measured radiances. Therefore a straight line was fitted to the data as

$$T_{\mathrm{B}}^{\mathrm{fit}} = a * T_{\mathrm{B}}^{\mathrm{ARTS}} + b. \quad (5)$$

The coefficients a and b, as well as their uncertainties (standard deviations), can be easily obtained from a least squares fit, using the error model as described above. The result is displayed in Figure 9 as a dashed line. The most significant deviation of the slope from unity is found for channel 18 (leftmost plot of Figure 9). This finding is persistent for all satellites and time periods, as we shall see below.

4. Results and Discussion

4.1. Comparison of Different Data Versions

[41] Table 3 shows comparison results for the three different Lindenberg data versions HRC, HRNC, and LRC, as defined in section 2.1. For simplicity, the comparison is limited to the 2002 time period for the satellite NOAA 15. Shown are σ_D and bias B, as well as slope a and offset b of the straight line fit, as defined in section 3.5.

[42] For surface channels 16 and 17 (not shown) there are no significant differences between the data versions, as expected. For humidity channels 18–20 there are differences, which increase with sounding altitude (from channels 20–18). For channel 18 the difference in B between HRC and HRNC data is 0.7 K, while the standard deviation of B is only 0.1 K. The HRC simulated radiances are colder than the HRNC ones, consistent with the fact that the HRC data are more humid than the HRNC data. The observed 0.7-K value of the difference is also roughly consistent with the average 3.4 %RH difference in UTH (9.6% relative difference) between these two data versions. From Figure 11 the expected value for the difference would have been 0.96 K, and the difference can be explained by the fact that the humidity bias between the two data

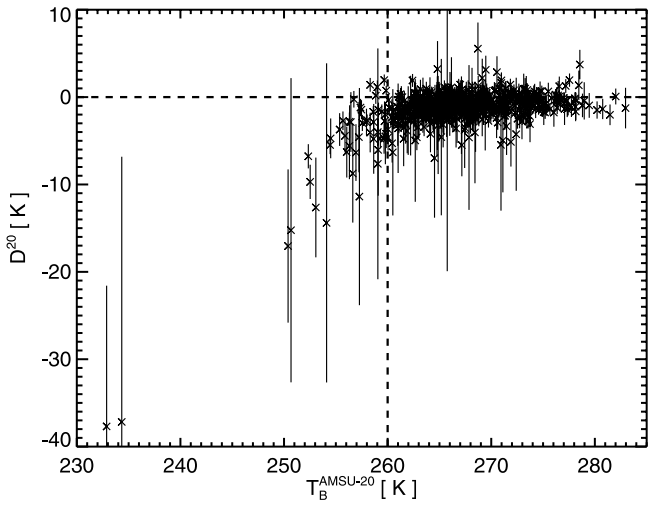

Figure 10. Measured minus modeled radiances for channel 20 (D^{20}) as a function of measured channel 20 radiance ($T_{\mathrm{B}}^{\mathrm{AMSU-20}}$). Time period, 2001–2002; satellite, NOAA 15. The vertical line at $T_{\mathrm{B}}^{\mathrm{AMSU-20}} = 260$ K indicates the cloud filter threshold. Data with lower $T_{\mathrm{B}}^{\mathrm{AMSU-20}}$ is discarded, not only for channel 20, but also for the other channels.

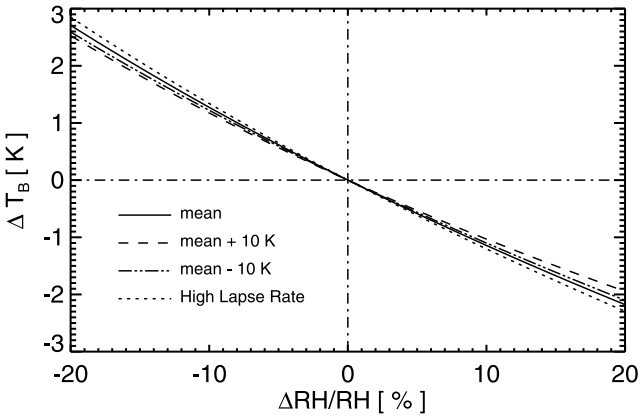

Figure 11. Sensitivity of simulated radiance for channel 18 to relative changes in relative humidity. Four temperature profiles were constructed using the mean Lindenberg temperature profile of 2002: the mean profile itself (solid line), the mean profile plus 10 K at all levels (dashed line), the mean profile minus 10 K at all levels (dash-dotted line), and the mean profile with a higher lapse rate below the tropopause (dotted line). The high-lapse-rate case had the same tropopause temperature but a 20-K-higher surface temperature. All four profiles have 50 %RH at all levels. Each profile was perturbed to a maximum of 20% on either side in 1% steps.

versions was computed over all radiosonde launches, whereas the brightness temperature bias was computed only over the launches that matched the satellite overpass.

[43] This result confirms that the satellite measurement is sensitive and accurate enough to distinguish between corrected and uncorrected data. Furthermore, the fact that the largest difference is found for the channel with the highest sounding altitude is consistent with the fact that the radiosonde correction algorithm has its highest impact in the upper troposphere.

[44] For the LRC data, on the other hand, the difference in B compared that of to the HRC data is much smaller and not significant compared to the standard deviation of B. This confirms that the vertical resolution of the LRC data is sufficient to accurately predict AMSU radiances, which can be explained by the approximately 3-km width of the AMSU Jacobians (see Figure 4). This is a very encouraging result, because it confirms that the wealth of low-resolution radiosonde data in the operational archives can be used for future intercomparison studies.

4.2. Comparison of Different Satellites and Time Periods

[45] The top data block in Table 4 shows comparison results broken down by satellite (NOAA 15 and 16) and time period (2001 and 2002). The number of matches in the different cases was as follows: 247 for NOAA 15 in 2001, 290 for NOAA 15 in 2002, 113 for NOAA 16 in 2001, and 154 for NOAA 16 in 2002. The first thing noticeable is that there is a small but significant difference between NOAA 15 and 16. To get an error estimate for this, the 2-year study time period was broken down further into subperiods of three months, yielding eight values each for σ_D, B, a, and b. From these, mean values and standard deviations of the difference between the two satellites were calculated, which are also displayed in Table 4.

[46] Thus significant differences between the two satellites are found for channels 18 and 19. These are the channels for which instrument performance has improved from NOAA 15 to 16; however, it is not clear how that translates into a systematic difference, since the variability σ_D of the difference D is dominated by atmospheric inhomogeneity, rather than instrument noise. So, it appears that the calibration has also slightly changed for these channels between the satellite versions.

4.3. Possible Explanations for the Slope in Channel 18

[47] The data in Tables 3 and 4 show that radiosonde humidity data and AMSU radiances are overall in very good agreement, with the notable exception of channel 18, which has a slope a significantly deviating from 1. The value ranges from 0.853 ± 0.024 K/K to 0.895 ± 0.027 K/K, depending on satellite and year. (Channel 19 also shows a slope, but the deviation from unity is barely significant.) There are three possible explanations for this discrepancy: (1) a systematic error in the RT model, (2) a systematic slope-like error in the AMSU radiances, and (3) a systematic error in the radiosonde data, increasing with lower humidity values.

[48] Possibility 1 can be easily studied by reprocessing the data with various perturbed RT model parameters. Likely candidate parameters are (1) the air-broadening parameter of the water vapor line, (2) the line intensity, (3) the temperature exponent of the air-broadening parameter, and (4) the water vapor continuum. Table 5 shows a summary of the results of these simulations. Although the perturbations were chosen quite large (20% for the intensity, 50% for the other parameters), none of the candidate parameters can bring the slope a close to unity. Higher perturbations cannot be justified on the basis of current spectroscopic knowledge and would also destroy the good agreement in the other channels. We can thus rule out possibility 1, the RT algorithm, as a source of the discrepancy, leaving only possibilities 2 and 3.

[49] Possibility 2, a slope-like error in the AMSU 18 radiances, is possible, but not very likely, given that the

Table 3. AMSU Versus Radiosonde Simulated Radiances for Different Versions of the Radiosonde Data[a]

Channel	Data Version	σ_D, K	B, K	a, K/K	b, K
18	HRC	1.6	−0.43 ± 0.11	0.850 ± 0.024	36.6 ± 5.9
18	HRNC	1.6	−1.11 ± 0.11	0.864 ± 0.024	32.4 ± 6.0
18	LRC	1.7	−0.32 ± 0.11	0.853 ± 0.024	35.9 ± 5.9
19	HRC	1.9	0.41 ± 0.10	0.908 ± 0.021	24.2 ± 5.4
19	HRNC	1.9	0.11 ± 0.10	0.921 ± 0.021	20.6 ± 5.5
19	LRC	2.0	0.40 ± 0.10	0.903 ± 0.021	25.4 ± 5.4
20	HRC	1.3	−0.91 ± 0.08	0.983 ± 0.019	3.8 ± 5.2
20	HRNC	1.3	−1.03 ± 0.08	0.986 ± 0.019	2.6 ± 5.2
20	LRC	1.3	−0.91 ± 0.08	0.973 ± 0.019	6.4 ± 5.1

[a]Time period, 2002; satellite, NOAA 15. The first column indicates the instrument channel, and the second column indicates the radiosonde data version: high-resolution corrected (HRC), high-resolution not corrected (HRNC), and low-resolution corrected (LRC, see section 2.1). The third column gives the standard deviation σ_D of the brightness temperature difference D as defined in section 3.5. All other quantities as defined in section 3.5.

Table 4. AMSU Versus Radiosonde Simulated Radiances for Different Satellites and Time Periods[a]

Channel	Data Set	σ_D, K	B, K	a, K/K	b, K
			Original Radiosonde		
18	N15, 2001	1.4	0.10 ± 0.12	0.888 ± 0.025	27.7 ± 6.0
18	N15, 2002	1.7	−0.32 ± 0.11	0.853 ± 0.024	35.9 ± 5.9
18	N16, 2001	1.6	−0.73 ± 0.14	0.895 ± 0.027	25.3 ± 6.7
18	N16, 2002	1.7	−1.15 ± 0.12	0.863 ± 0.027	32.8 ± 6.6
18	N15-N16	0.0 ± 0.2	0.99 ± 0.55	−0.020 ± 0.060	5.8 ± 14.9
19	N15, 2001	1.7	0.10 ± 0.10	0.953 ± 0.021	12.3 ± 5.5
19	N15, 2002	2.0	0.40 ± 0.10	0.903 ± 0.021	25.4 ± 5.4
19	N16, 2001	1.3	−0.66 ± 0.13	0.923 ± 0.026	19.5 ± 6.8
19	N16, 2002	1.5	−0.98 ± 0.12	0.926 ± 0.028	18.4 ± 7.3
19	N15-N16	0.5 ± 0.2	1.06 ± 0.60	0.009 ± 0.100	−1.3 ± 26.2
20	N15, 2001	1.2	−0.97 ± 0.09	1.037 ± 0.020	−10.9 ± 5.5
20	N15, 2002	1.3	−0.91 ± 0.08	0.973 ± 0.019	6.4 ± 5.1
20	N16, 2001	1.2	−0.98 ± 0.13	0.959 ± 0.030	10.0 ± 8.0
20	N16, 2002	1.4	−1.20 ± 0.12	0.945 ± 0.025	13.6 ± 6.8
20	N15-N16	−0.1 ± 0.2	0.09 ± 0.37	0.009 ± 0.133	−2.5 ± 35.4
			Radiosonde +2 %RH at 0 %RH		
18	N15, 2001	1.4	0.57 ± 0.12	0.938 ± 0.026	15.9 ± 6.4
18	N15, 2002	1.6	0.18 ± 0.11	0.904 ± 0.026	23.6 ± 6.3
18	N16, 2001	1.5	−0.19 ± 0.14	0.957 ± 0.029	10.3 ± 7.1
18	N16, 2002	1.6	−0.62 ± 0.12	0.919 ± 0.028	19.3 ± 7.0
19	N15, 2001	1.6	0.35 ± 0.10	0.986 ± 0.022	4.0 ± 5.6
19	N15, 2002	1.9	0.68 ± 0.10	0.940 ± 0.022	16.3 ± 5.6
19	N16, 2001	1.2	−0.35 ± 0.13	0.964 ± 0.028	9.0 ± 7.1
19	N16, 2002	1.4	−0.68 ± 0.12	0.967 ± 0.029	8.0 ± 7.7
20	N15, 2001	1.2	−0.85 ± 0.09	1.055 ± 0.021	−15.7 ± 5.6
20	N15, 2002	1.3	−0.79 ± 0.08	0.994 ± 0.020	0.8 ± 5.3
20	N16, 2001	1.1	−0.82 ± 0.13	0.979 ± 0.030	4.8 ± 8.2
20	N16, 2002	1.4	−1.05 ± 0.12	0.971 ± 0.026	6.7 ± 7.0
			Radiosonde +4 %RH at 0 %RH		
18	N15, 2001	1.4	1.06 ± 0.12	0.995 ± 0.028	2.4 ± 6.8
18	N15, 2002	1.5	0.69 ± 0.11	0.961 ± 0.027	10.2 ± 6.7
18	N16, 2001	1.5	0.37 ± 0.14	1.024 ± 0.031	−5.6 ± 7.6
18	N16, 2002	1.5	−0.07 ± 0.12	0.983 ± 0.030	4.2 ± 7.5
19	N15, 2001	1.4	1.06 ± 0.12	0.995 ± 0.028	2.4 ± 6.8
19	N15, 2002	1.9	0.98 ± 0.10	0.979 ± 0.023	6.5 ± 5.9
19	N16, 2001	1.2	−0.01 ± 0.13	1.008 ± 0.029	−2.2 ± 7.5
19	N16, 2002	1.4	−0.36 ± 0.12	1.011 ± 0.031	−3.2 ± 8.0
20	N15, 2001	1.2	−0.71 ± 0.09	1.075 ± 0.021	−20.9 ± 5.7
20	N15, 2002	1.3	−0.64 ± 0.08	1.017 ± 0.020	−5.3 ± 5.4
20	N16, 2001	1.2	−0.65 ± 0.13	1.000 ± 0.031	−0.5 ± 8.3
20	N16, 2002	1.4	−0.89 ± 0.12	0.999 ± 0.027	−0.6 ± 7.2

[a]The second column indicates the satellite and time period; the satellite is either NOAA 15 or NOAA 16, and the time period is the whole year of either 2001 or 2002. The radiosonde data version is LRC. All other quantities are as defined in section 3.5. The table contains three blocks of data: at the top, original radiosonde data; in the middle, radiosonde data increased by 2 %RH at 0 %RH; and at the bottom, radiosonde data increased by 4 %RH at 0 %RH. For the original radiosonde data an additional row for each channel gives an estimate of the difference between the two satellites (mean value and standard deviation, see text for details).

Table 5. NOAA 15, 2001[a]

Channel	Data Version	σ_D, K	B, K	a, K/K	b, K
18	LRC	1.4	0.10 ± 0.12	0.888 ± 0.025	27.7 ± 6.0
18	LW − 50%	1.6	−0.76 ± 0.12	0.902 ± 0.025	23.4 ± 6.3
18	LI + 20%	1.4	1.94 ± 0.12	0.903 ± 0.025	25.6 ± 6.1
18	Tx − 50%	1.4	0.16 ± 0.12	0.890 ± 0.025	27.1 ± 6.1
18	WC + 50%	1.4	0.15 ± 0.12	0.888 ± 0.025	27.5 ± 6.1
19	LRC	1.7	0.10 ± 0.10	0.953 ± 0.021	12.3 ± 5.5
19	LW − 50%	1.9	−3.85 ± 0.10	0.979 ± 0.022	1.8 ± 5.8
19	LI + 20%	1.7	1.62 ± 0.10	0.940 ± 0.021	17.0 ± 5.3
19	Tx − 50%	1.7	−0.22 ± 0.10	0.958 ± 0.021	10.7 ± 5.5
19	WC + 50%	1.7	0.27 ± 0.10	0.951 ± 0.021	12.9 ± 5.4
20	LRC	1.2	−0.97 ± 0.09	1.037 ± 0.020	−10.9 ± 5.5
20	LW − 50%	2.0	−3.90 ± 0.09	0.860 ± 0.018	34.1 ± 4.8
20	LI + 20%	1.2	0.09 ± 0.09	1.054 ± 0.021	−14.3 ± 5.5
20	Tx − 50%	1.2	−1.21 ± 0.09	1.036 ± 0.020	−11.0 ± 5.5
20	WC + 50%	1.2	−0.42 ± 0.09	1.051 ± 0.021	−14.1 ± 5.5

[a]LRC, low-resolution corrected radiosonde data, H2O model default parameters. LW − 50%, air-broadening parameter scaled by −50%; LI + 20%, line intensity scaled by +20%; Tx − 50%, temperature exponent of air broadening parameter scaled by −50%; WC + 50%, water vapor continuum scaled by +50%.

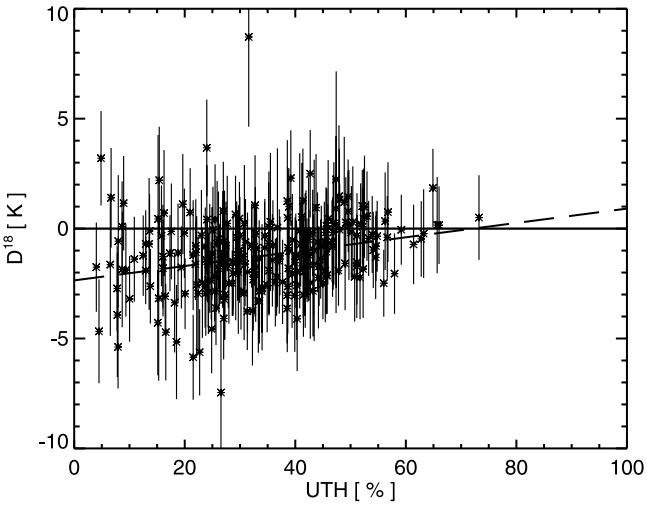

Figure 12. Measured minus modeled radiances for channel 18 (D^{18}) as a function of UTH for the year 2002 and for NOAA 16. The dashed line represents a linear fit between UTH and D^{18}, taking into account the error model described in section 3.3. The fitted line in this case has a slope of 0.033 K/%RH and an offset of −2.4 K. The slope and offset for other years and satellites vary between 0.014 and 0.038 K/%RH and between −0.6 and −2.4 K, respectively.

slope is remarkably stable between the two different satellites studied, and given also that from the point of view of the radiometer this channel is not significantly different from any other channel. What really distinguishes channel 18 from the other humidity channels is its high atmospheric sounding altitude around 6–10 km, an altitude where radiosondes are most challenged. Thus the results indicate that even the corrected Lindenberg data may still underestimate the humidity for very dry conditions.

[50] To quantify this underestimation, D^{18} was plotted as a function of UTH (average RH between 500 and 200 hPa), and a straight line was fitted (Figure 12). This yields at 0 %RH a brightness temperature difference of −(0.6–2.4) K, depending on satellite and year. To compensate for this, the true UTH would have to be approximately 2–4 %RH where the radiosonde shows 0 %RH, according to Figure 11.

[51] To verify this assertion, a simple linear correction was applied to the radiosonde humidity data. The correction was +2 %RH at 0 %RH, decreasing linearly to 0 %RH at 70 %RH. Then the intercomparison was repeated with the modified radiosonde data. This indeed brings the slope in channel 18 (and 19) closer to unity, while conserving the good agreement in channel 20, as shown in the second part of Table 4. Repeating the exercise with a larger correction of +4 %RH at 0 %RH (third part of Table 4) leads to a slight overcorrection with slopes more often above 1 than below. The necessary correction to the radiosonde data therefore seems to be between +2 and +4 %RH at 0 %RH.

5. Summary and Conclusions

[52] A robust method to compare radiosonde humidity data to AMSU data was developed, which is planned to be used for future global studies. The new method has some unique features: First, the comparison is done for a target area, allowing an estimation of the atmospheric variability. Second, displacement and cloud filters are applied. Third, a complete and consistent error model is used.

[53] The method was validated by a detailed case study, using the high-quality Lindenberg radiosonde data and the NOAA 15 and 16 satellite data for the time period from 2001 to 2002. The study confirmed that low-vertical-resolution data, as found in operational archives, are sufficient to accurately predict AMSU radiances. However, it also demonstrated that corrections applied in Lindenberg to the standard Vaisala data processing make a significant difference, particularly in the upper troposphere.

[54] Overall, the AMSU data are in very good agreement with the radiosonde data, with the notable exception of a slope in channel 18. By reprocessing with perturbed RT model parameters, RT model error was ruled out as a possible explanation for the slope, leaving only AMSU data and radiosonde data. Of these two, the latter seem the more likely explanation, which would mean that the corrected Lindenberg radiosonde data have a small residual dry bias at low humidities, giving 0 %RH when the true humidity is still approximately 2–4 %RH.

[55] **Acknowledgments.** Thanks to Nigel Atkinson from the Met Office, UK, for providing AMSU noise equivalent temperature data from the operational calibration procedure. Thanks also to the British Atmospheric Data Centre (BADC) for giving us access to radiosonde data from stations worldwide. Special thanks to Lisa Neclos from the Comprehensive Large Array-Data Stewardship System (CLASS) of the U.S. National Oceanic and Atmospheric Administration (NOAA) for providing the AMSU data. Thanks to Brian Soden, NOAA Geophysical Fluid Dynamics Laboratory, Princeton, for discussions, and to Patrick Eriksson, Chalmers University, Gothenburg, for discussions and comments on the manuscript. Furthermore, thanks to the ARTS radiative transfer community, many of whom have indirectly contributed by implementing features of the ARTS model. In particular, thanks to Thomas Kuhn, now at the University of Cologne, for implementing absorption continua. Finally, we would also like to thank the two reviewers for their valuable comments. This study was funded by the German Federal Ministry of Education and Research (BMBF), within the AFO2000 project UTH-MOS, grant 07ATC04. It is a contribution to COST Action 723 "Data Exploitation and Modeling for the Upper Troposphere and Lower Stratosphere."

References

Atkinson, N. C. (2000), Calibration, monitoring and validation of AMSU-B, paper presented at A0.2 Symposium of the 33rd COSPAR Scientific Assembly, Comm. on Space Res., Warsaw, July. (Reproduced in *Adv. Space Res.*, *28*, 117–126, 2001.)

Bates, J. J., D. L. Jackson, F.-M. Breon, and Z. D. Bergen (2001), Variability of tropical upper tropospheric humidity 1979–1998, *J. Geophys. Res.*, *106*(D23), 32,271–32,281.

Buehler, S. A., P. Eriksson, T. Kuhn, A. von Engeln, and C. Verdes (2004), ARTS, the atmospheric radiative transfer simulator, *J. Quant. Spectrosc. Radiat. Transfer*, in press.

Chevallier, F. (2001), Sampled databases of 60-level atmospheric profiles from the ECMWF analysis, *Res. Rep. 4*, Satell. Appl. Facil. Program, EUMETSAT-ECMWF, Reading, England.

Elliot, W. P., and D. J. Gaffen (1991), On the utility of radiosonde humidity archives for climate studies, *Bull. Am. Meteorol. Soc.*, *72*, 1507–1520.

Engelen, R. J., and G. L. Stephens (1998), Comparison between TOVS/HIRS and SSM/T-2 derived upper tropospheric humidity, *Bull. Am. Meteorol. Soc.*, *79*, 2748–2751.

Harries, J. E. (1997), Atmospheric radiation and atmospheric humidity, *Q.J.R. Meteorol. Soc.*, *123*, 2173–2186.

Leiterer, U., H. Dier, and T. Naebert (1997), Improvements in radiosonde humidity profiles using RS80/RS90 radiosondes of Vaisala, *Beitr. Phys. Atmos.*, *70*(4), 319–336.

Press, W. H., S. A. Teukolsky, W. T. Vetterling, and B. P. Flannery (1992), *Numerical Recipes in C*, 2nd ed., Cambridge Univ. Press, New York.

Reale, A. L., M. Chalfant, A. Allegrino, F. Tilley, M. Ferguson, and M. Pettey (2003), Advanced-TOVS (ATOVS) sounding products from

NOAA polar-orbiting environmental satellites, paper presented at 12th AMS Conference on Satellite Meteorology and Oceanography, Am. Meteorol. Soc., Long Beach, Calif., 9–13 Feb.

Rodgers, C. D. (2000), *Inverse Methods for Atmospheric Sounding: Theory and Practise*, 1st ed., World Sci., River Edge, N. J.

Rosenkranz, P. W. (1993), Absorption of microwaves by atmospheric gases, in *Atmospheric Remote Sensing by Microwave Radiometry*, edited by M. A. Janssen, pp. 37–90, John Wiley, Hoboken, N. J.

Rosenkranz, P. W. (1998), Water vapor microwave continuum absorption: A comparison of measurements and models, *Radio Sci.*, *33*(4), 919–928. (Correction, *Radio Sci.*, *34*, 1025, 1999.)

Saunders, R. W., T. J. Hewison, S. J. Stringer, and N. C. Atkinson (1995), The radiometric characterization of AMSU-B, *IEEE Trans. Microwave Theory Tech.*, *43*(4), 760–771.

Soden, B. J., and F. P. Bretherton (1993), Upper tropospheric relative humidity from the GOES 6.7 μm channel: Method and climatology for July 1987, *J. Geophys. Res.*, *98*(D9), 16,669–16,688.

Soden, B. J., and J. R. Lanzante (1996), An assessment of satellite and radiosonde climatologies of upper-tropospheric water vapor, *J. Clim.*, *9*, 1235–1250.

Soden, B. J., D. D. Turner, B. M. Lesht, and L. M. Miloshevich (2004), An analysis of satellite, radiosonde, and lidar observations of upper tropospheric water vapor from the Atmospheric Radiation Measurement Program, *J. Geophys. Res.*, *109*, D04105, doi:10.1029/2003JD003828.

Spencer, R. W., and W. D. Braswell (1997), How dry is the tropical free troposphere? implications for global warming theory, *Bull. Am. Meteorol. Soc.*, *78*, 1097–1106.

Sreerekha, T. R., S. A. Buehler, and C. Emde (2002), A simple new radiative transfer model for simulating the effect of cirrus clouds in the microwave spectral region, *J. Quant. Spectrosc. Radiat. Transfer*, *75*, 611–624.

S. A. Buehler, V. O. John, and M. Kuvatov, Institute of Environmental Physics, University of Bremen, Otto-Hahn-Allee 1, D-28359 Bremen, Germany. (sbuehler@uni-bremen.de; vojohn@uni-bremen.de; kmashrab@uni-bremen.de)

H. Dier and U. Leiterer, Meteorological Observatory Lindenberg, German Weather Service, Am Observatorium 12, D-15864 Lindenberg, Germany. (horst.dier@dwd.de; ulrich.leiterer@dwd.de)